AuxPdy based heterogeneous nanocatalysts for plasmonmediated enhanced catalysis under visible light irradiation

(Article begins on next page)

26 December 2024

FULL PAPER

Au_xPd_y-based heterogeneous nanocatalysts for plasmon-mediated enhanced catalysis under visible light irradiation

Priyanka Verma,[a,b,c]* Panashe M. Mhembere,[b] Paolo Tallone,[d,e] Maela Manzoli,[d] Giuseppina Cerrato,[f] Ryo Watanabe,[c] Choji Fukuhara,[c] Robert Raja[b]* and Hiromi Yamashita[a]*

Abstract: The formation of hybrid plasmonic nanocatalysts made of Au nanoparticles (NPs) combined with catalytically active NPs has gained great attention owing to their interesting properties and efficient catalysis under visible light irradiation. However, the research on the combination of plasmonic metal NPs with unique support frameworks is still limited. In this report, the varying ratio of Au_xPd_y prepared by the extrusion method on the CuCIP framework has been correlated to its optimized catalysis in the Suzuki-Miyaura coupling reaction in dark and under visible light irradiation. The prepared catalysts Au_xPd_y/CuCIP were characterized by spectroscopic techniques to understand the structural and electronic modification with different metal ratios. The presence of bimetallic NPs on the surface was confirmed by HR-TEM measurements and $[MCl_4]^{n-}$ species in the framework were validated by XPS, FT-EXAFS, DR UV-Vis-NIR, and Raman analysis. The obtained results display the superior catalytic performance and highest plasmonic enhancement factor over Au_1Pd_1/CuCIP under visible light irradiation, which was facilely recycled and reused for several cycles. The hot-electron transfer mechanism has been discussed for enhanced catalysis in the plasmon-driven Suzuki−Miyaura coupling reaction. These results are highly significant in the rational design of new plasmonic photocatalysts combined with unique support materials.

[a]   Dr. P. Verma, Prof. H. Yamashita
        Division of Materials and Manufacturing Science, Graduate School of Engineering, Osaka University, 2-1 Yamadaoka, Suita, Osaka 565-0871, Japan
        E-mail: yamashita@mat.eng.osaka-u.ac.jp

[b]   Dr. P. Verma, P.M. Mhembere, Prof. R. Raja
        School of Chemistry, University of Southampton, University Road, Highfield, Southampton, SO17 1 BJ, United Kingdom
        E-mail: r.raja@soton.ac.uk

[c]   Dr. P. Verma, Prof. R. Watanabe, Prof. C. Fukuhara
        Department of Applied Chemistry and Biochemical Engineering, Faculty of Engineering, Shizuoka University, 3-5-1, Johoku, Naka-ku, Hamamatsu, Shizuoka 432-8561, Japan
        E-mail: verma.priyanka@shizuoka.ac.jp

[d]   P. Tallone, Prof. M. Manzoli
        Department of Drug Science and Technology, NIS Center and INSTM Reference Center, University of Torino, Via P. Giuria 9, 10125, Torino, Italy

[e]   P. Tallone
        Applied Science and Technology Department, Politecnico di Torino, C. so Duca degli Abruzzi 24, Torino 10129, Italy

[f]   Prof. G. Cerrato
        Department of Chemistry, University of Turin, Via Pietro Giuria 7, 10125 Turin, Italy

        Supporting information for this article is given via a link at the end of the document.

Introduction

Plasmonic catalysis is rapidly emerging in the field of heterogeneous photocatalysis to exploit the unique optical absorption property of noble metal nanostructures such as Ag and Au. These nanostructured materials are capable of harvesting abundant sunlight and converting it into chemical energy owing to their unique visible light absorption because of localized surface plasmon resonance (LSPR).[1–3] LSPR is defined as the collective oscillation of free electrons to establish resonance between photons of the incident light and the natural frequency of surface electrons in nanoparticles (NPs).[4] Recently, these plasmonic metal nanostructures are being studied in combination with other active metal species, for example, Pd, Ru, Ni, and Pt in order to improve their catalytic and optical properties.[5] In the last decade, plasmon-mediated heterogeneous catalysis was explored in several important catalytic reactions to improve the product yield under mild reaction conditions such as hydrogen generation[6–9], CO_2 reduction[10,11], water purification[12] and carbon-carbon coupling reaction.[13–16]

The immobilization of these novel plasmonic nanostructures has been reported on a variety of support materials ranging from insulator mesoporous-macroporous silica to semiconducting TiO_2 and metal-organic frameworks (MOFs).[1,17–20] However, the use of copper chloropyrophosphate (CuCIP) as the support material for plasmonic nanoparticles (NPs) has not been reported in the literature yet. CuCIP materials are emerging as a robust platform for the generation and anchoring of NPs of several noble metals.[21] The framework is composed of halide ions and a lower charge density of Cu^{II}, which assists in the ionic mobility of the system. The chloride ions are present at the apex of $4 \times CuO_4Cl$ square-based pyramids and pyrophosphate (P_2O_7) units that link the quartets to form 1D channels 12.7 Å in diameter. The charge compensation is done by the Rb^+ cations and tetrachloro metallate anions such as $[CuCl_4]^{2-}$, $[AuCl_4]^-$, $[PdCl_4]^{2-}$ or $[PtCl_4]^{2-}$ present within the microporous channels. The presence of these metal complexes facilitates the generation of nano-sized, uncapped metal NPs by undergoing H_2 reduction at higher temperatures, a novel process called as extrusion method. This treatment leads to the extrusion of metallic species moving towards the material's surface to form uniformly distributed metal NPs by releasing HCl and RbCl as the by-product to preserve the neutrality of the framework. The extrusion process is possible owing to the 1D micropores present within the framework (**Figure 1**). Hence, the design and development of hybrid materials that can assist in the controlled formation of active metal NPs and display plasmonic characteristics on a chemically diverse porous phosphate material can prove to be a unique approach to synthesize supported metal NPs for catalytic and photocatalytic applications. It has already been reported in the literature on the use of monometallic M/CuCIP to display a high catalytic response in the selective oxidation of industrially important alcohols such

as benzyl, vanillyl, and KA oil.[22–24] In the present report, we have investigated the extrusion of AuPd bimetallic NPs capable of displaying plasmonic properties for their application in the organic coupling reaction under visible light irradiation.
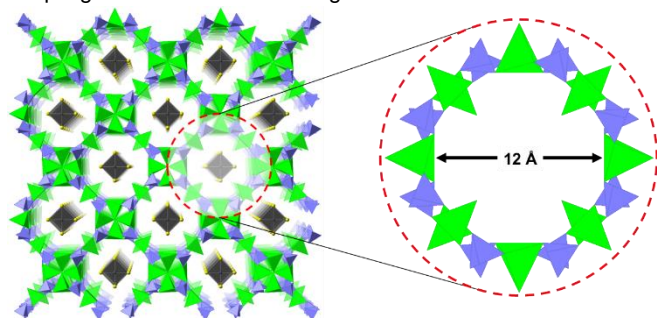

Figure 1. The 1D microporous architecture of the CuClP framework, with the $[MCl_4]^{n-}$ anions (grey polyhedra) present within the micropores. Charge balancing ions are omitted for clarity.

Prior investigations of the CuClP materials saw them used exclusively for alcohol oxidation reactions, where they showed varying degrees of activity depending on the metal NP.[21] On the other hand, the Pd/CuClP catalyst has been side-lined largely due to its limited stability under activation conditions, which results in the sintering of the framework.[23] Presented here is an avenue toward remedying the limited stability of the Pd/CuClP system. The approach taken here is by exploiting the higher stability of the Au/CuClP catalyst under activation conditions, which exceeds that of the Pd analogue. This would be done by the synthesis of a bimetallic system, incorporating both Au and Pd in the CuClP framework.

In the present report, the Au_xPd_y/CuClP catalysts have been explored for their potential application in Suzuki-Miyaura coupling reactions in dark and under visible light irradiation conditions. This bimetallic combination has been reported to display superior product yields with significant plasmonic enhancement.[25–27] The Suzuki-Miyaura was chosen as a model reaction, since it is crucial in the synthesis of various key industrial products including pharmaceuticals. In this reaction, an organoboron compound and an organic halide are generally coupled in a Pd-catalyzed process to form the required C-C bonds. Owing to the wide range of industrial applications of the Suzuki coupling reaction, there has been a strong imperative to understand its catalytic mechanism.[28] This has led to a catalytic cycle that indicates the well-established key steps and intermediates in the reaction. We observed different reaction rates on varying the composition ratio of Au and Pd in the CuClP framework. Interestingly, the reaction rates were found to be enhanced in the presence of light irradiation conditions for the bimetallic catalyst. Furthermore, the stability tests by catalysis and characterization revealed the reusability and preservation of structural crystallinity in Au_xPd_y/CuClP catalysts.

Results and Discussion

Structural characterization of CuClP and Au_xPd_y/CuClP catalysts

The powder X-ray diffraction (XRD) analysis of the Au_xPd_y/CuClP catalysts before (**Figure 2a**) and after (**Figure 2b**) the activation process showed that the fresh (as-synth) catalysts had the expected tetragonal phase associated with the successful formation of the CuClP framework. Similarly, the activated catalysts did not show any additional phases. Crucially, this was only true for the Au-containing CuClP catalysts; the monometallic Pd/CuClP showed the expected sintering. This was confirmed by the accompanying formation of rubidium polyphosphate phases (as shown by the grey bars in **Figure 2b**). The formation of alternative phosphate phases was contingent upon the reorganization of the pyrophosphate groups in the framework, which played an integral role in maintaining the porous structure of the CuClP framework. This reorganization was evident only in the monometallic Pd catalyst.

The XRD results were evidence for the theorized stabilization of the Pd/CuClP system via the incorporation of Au. Ordinarily, the high affinity of the $[PdCl_4]^{2-}$ moieties for the parent framework results in the sintering of the framework before successful extrusion of the Pd anions, even at a relatively low activation temperature of 200 °C.[23] In contrast, the Au system is stable at such temperatures, with the CuClP framework remaining unchanged at 200 °C. This feature of the Au system was surmised to be intrinsic to the $[AuCl_4]^-$ anions, meaning that the incorporation of these anions into the Pd systems served to create discrete regions of stability within the framework, with a more stable structure achieved overall.

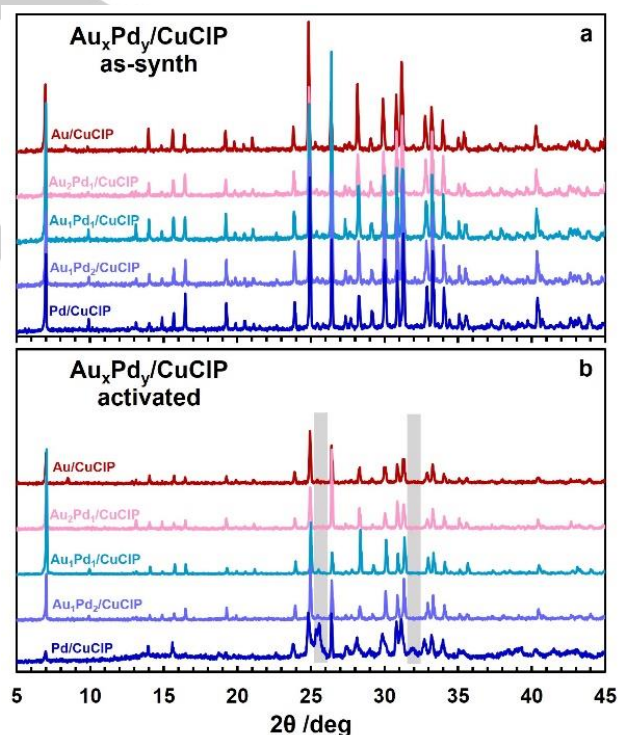**Figure 2.** XRD patterns of Au_xPd_y/CuClP catalysts (a) as-synthesized and (b) after activation. Grey bars indicate some of the reflections that are associated with rubidium polyphosphate phases.

Figure 3 shows the X-ray photoelectron spectroscopy (XPS) data for the activated Au_xPd_y/CuClP catalysts, separated into the Au

and Pd regions. The C1s, P2p, and Cu2p XPS spectra are shown in **Figure S1**. After activation of the monometallic Au/CuClP catalyst, there was a considerable amount of Au^0 at the surface of the framework.
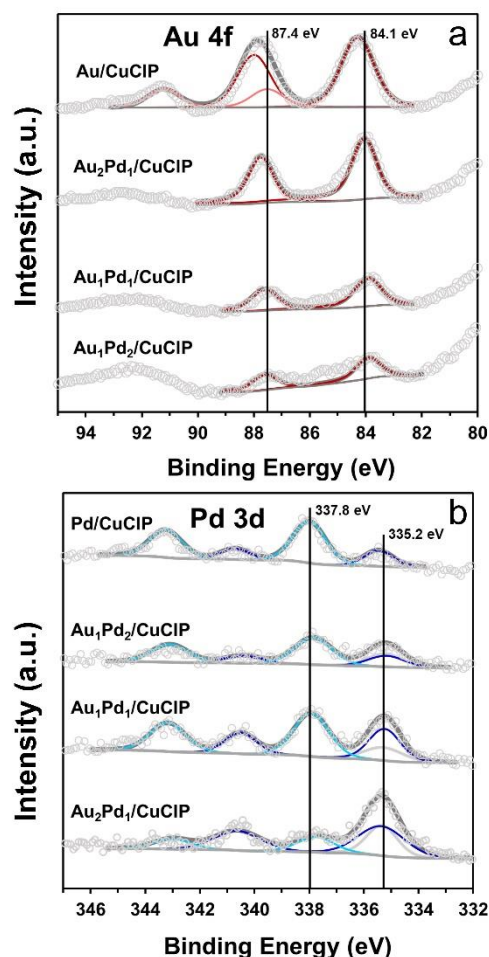

Figure 3. XPS spectra of the Au_xPd_y/CuClP catalysts after activation; (a) Au region and (b) Pd region. NB grey component overlapping the Pd^0 $3d_{5/2}$ component in the bimetallic catalysts is due to Au^0 $4d_{5/2}$.

Some Au^{3+} was also present; suggesting that there was an incomplete reduction of the $[AuCl_4]^-$ precursor during the activation process. Furthermore, the binding energy of the Au^0 component occurred at 84.1 eV (grey line in **Figure 3**a); similar to bulk Au.[22,29] This observation suggested that the Au present in this catalyst was not in nanoparticulate form, as nanoscale Au had been documented to have a different binding energy from its bulk counterpart. Specifically, the Au^0 $4f^{7/2}$ binding energy of Au within NPs was known to occur at lower binding energy values (83.0-83.8 eV). This effect was associated with changes in the local density of states near the Fermi level of the nanoparticulate Au^0.[30]

The extrusion process was thought to generate particles with a narrow size distribution, as the amount of $[MCl_4]^{n-}$ anions within a micropore put a threshold on the number of possible M atoms that constituted each NP. In such a case, one would expect

signs of Au NPs in the XPS data, however, the reality was the opposite. This suggested that the Au^0 particles that were shown by the XPS were not formed via extrusion. This was not an unreasonable assumption, given that the synthetic procedure used in the preparation of these catalysts was a hydrothermal method. Hinde et al. theorized the possibility that some amount of the $[MCl_4]^{n-}$ anions would not be included in the micropores, but get deposited on the framework.[22] Reduction of such moieties would not occur in such a controlled manner as what would extrusion would allow, thus they would be larger and therefore possess electronic characteristics similar to those of Au NPs.

Interestingly, the Au^0 $4f_{7/2}$ binding energy in the bimetallic catalysts was lower than it was in the monometallic Au catalyst. This indicated the presence of a large proportion of Au^0 NPs on the surface of the CuClP framework that were smaller in size than those present on the surface of the monometallic catalyst. These smaller particles were surmised to have been formed via the intended extrusion process. This suggested that the presence of Pd facilitated the extrusion of Au at lower temperatures in the bimetallic catalyst than in the monometallic catalyst.

XPS data of the Pd (**Figure 3b**) state yielded interesting, albeit, expected results. The data showed a mix of Pd oxidation states, regardless of the presence of Au; similar to previous findings.[22] The peaks observed at B.E. of 335.0 eV and 336.7 eV are ascribed to the standard $3d_{5/2}$ Pd^0 and Pd^{2+} species, respectively. The most striking feature of the Pd catalysts was that the proportion of Pd^0 increased with the incorporation of Au in the bimetallic catalysts. The proportion of the Pd^{2+} component in the monometallic catalyst was 3.0 times more than that of the Pd^0 component. Conversely, the greatest proportion of Pd^{2+} among the bimetallic catalysts was 1.6 times more than Pd^0, which was observed in the Au_1Pd_1/CuClP catalyst. From a structural perspective, this alluded to the possibility that Au was playing a role in the generation of more Pd^0. Such an interaction could have been due to the presence of Au resulting in a co-reduction process, which induced a more efficient reduction of Pd during the activation process. [31,32]

X-ray absorption near-edge spectroscopy (XANES) was then used to gain insight into the nature of Au and Pd in the Au_xPd_y/CuClP catalysts upon reduction. Probing the Au L_3-edge of the Au_xPd_y/CuClP materials showed that the majority of the Au within the samples was similar to the $KAuCl_4$ standard (**Figure 4a**) in all bimetallic catalysts. This showed that the Au in the CuClP catalysts was still in the 1D micropores. The Au^0 evidenced by XPS was therefore only confined to the surface regions, with most of the Au remaining in its precursor form. This was not an unexpected observation, given the known stability of the Au/CuClP system. Indeed, it validated the supposition that the introduction of Au into the Pd/CuClP framework resulted in Au imparting stability to the framework. XANES spectra of the Pd K-edge of the Au_xPd_y/CuClP catalysts displayed similar information to that of the Au case; the Pd in the samples closely matched the chlorometallate salt. However, a difference in the edge intensity peaks could attribute to the presence of extruded metal NPs. Again, the Pd^0 evidenced by the XPS analysis was confined only to the surface regions.

From the XANES analysis, it was clear that much of the Au and the Pd in the Au_xPd_y/CuClP catalysts had remained in their non-metallic states. To further understand the local environment of Au

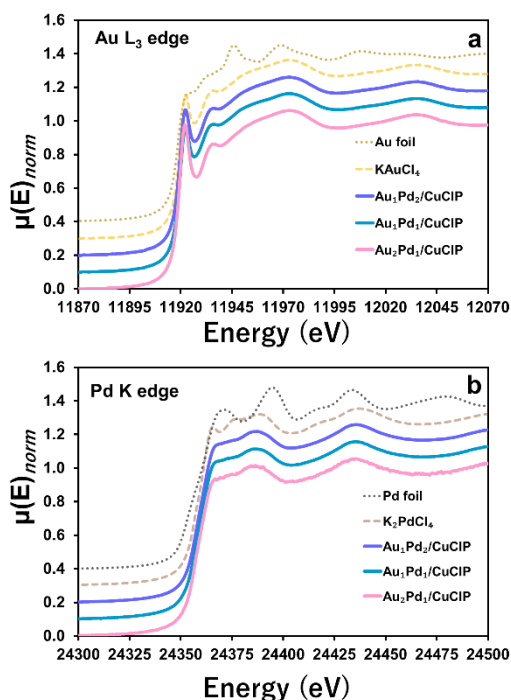and Pd, extended X-ray absorption fine structure (EXAFS) analysis was carried out (**Figure 5**).

Figure 4. XANES spectra of Au_xPd_y/CuClP catalysts at (a) the Au L_3-edge and (b) the Pd K-edge. Metallic foil and chlorometallate standards are shown for comparison.
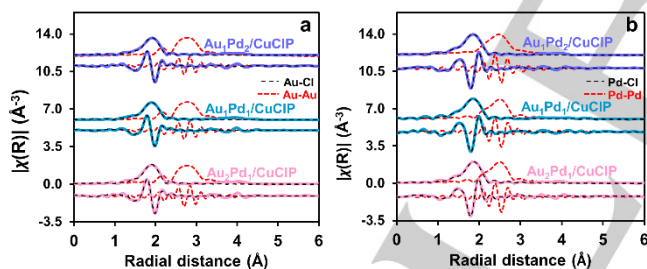

Figure 5. The magnitude and real component of the k^2 weighted Fourier transform of the EXAFS for the (a) Au edge and (b) Pd edge of Au_xPd_y/CuClP catalysts. Fitting parameters are provided in Table S2.

The first shell fits of the Au EXAFS for all the catalysts were compared with the $[AuCl_4]^-$ moiety in the framework and also with the Au foil. Overlaid fits (Figure 5a) show that the Au EXAFS closely matches the framework $[AuCl_4]^-$ across all the bimetallic catalysts. Therefore, a large fraction of Au in the bimetallic catalysts was reasonably still in the framework. Similarly, the Pd EXAFS showed good agreement between the data and the framework-bound $[PdCl_4]^{2-}$ anion.

The bulk analysis indicated that there was limited extrusion of the $[MCl_4]^{n-}$ anions from the CuClP framework, however, the surface was populated with a relatively large amount of metallic Au and Pd. Given that the BET surface area of the CuClP

materials was low (<5 m^2/g), the 1D micropores of the framework were not expected to be involved in the catalytic reaction. This meant that the coupling reaction could only take place at the surface of the CuClP framework. Thus, the surface characterization by XPS was the most relevant in the context of catalysis, while the XAS data provided information regarding the structural stability of the CuClP.

The NPs size and morphology of the support framework were investigated by FE-SEM and HR-TEM, as shown in **Figure 6**. The FE-SEM image of the Au_1Pd_1/CuClP displays a cuboid crystal and the formation of extruded roundish metal NPs (**Figure 6** (a,b)) appearing as white spots and rubidium phosphate (Rb_3PO_4) crystals with ramified morphology (**Figure 6**(b)). The energy dispersive X-ray spectroscopic (EDS) analysis revealed the existence of bimetallic AuPd NPs (**Figure S2).**

The HR-TEM analysis (**Figure 6** (c, d)) clearly displays the formation of uniformly dispersed small-sized NPs with an average particle size diameter of 4.2±1.3 nm (Figure 6 (f)). The bimetallic composition of NPs on CuClP was confirmed by the EDS analysis also in this case. The diffraction fringes typical of the long-range ordered structure of CuClP can also be seen in Figure 6 (d).

It is then possible to state that the Au NPs tended to aggregate to form large-size NPs which were also observed at some regions on the surface of the catalyst (**Figure 6** (a,b)). Conversely, the Pd-containing NPs were always small-sized and uniformly dispersed on the surface. It can be predicted that the extrusion process damaged some parts of the framework, leading to the formation of aggregated Au NPs. The EDS mapping result as shown in **Figure S3** also confirms the homogeneous distribution of Cu, Cl, and P.

The formation of such uniformly dispersed spherical NPs (< 5 nm) validates the effectiveness of the synthetic procedure by the extrusion method.
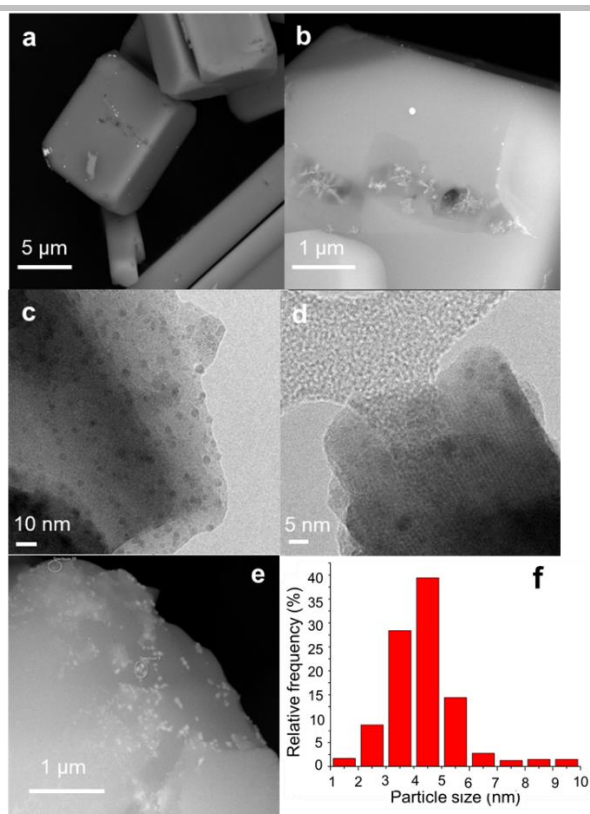
Figure 6. (a) FE-SEM BSE image of the Au_1Pd_1/CuCIP catalyst displaying the cuboid crystal, (b) FE-SEM BSE image with metal NPs and Rb_3PO_4 crystals, (c, d) HR-TEM images of Au_1Pd_1/CuCIP catalyst with metal NPs and diffraction fringes of the crystalline CuCIP framework, (e) FE-SEM BSE image of the re-used Au_1Pd_1/CuCIP catalyst and (f) particle size distribution based on the HR-TEM results.

As a matter of fact, the monometallic Au/CuCIP contained an homogeneous distribution of large-sized (18.13 ± 2.5 nm) Au NPs extruded from the framework (data not shown). Conversely, small-sized and well-dispersed metal NPs along with the presence of extruded Rb_3PO_4 crystals were observed on the monometallic Pd/CuCIP. Overall, the amount of extruded Rb_3O_4 crystals was found to increase upon increasing the Pd content in the CuCIP framework.

As for the bimetallic catalysts, the different ratios of Au and Pd led to different extents of NPs extrusion from the framework. In particular, the higher Pd content led to larger amounts of Rb_3PO_4 crystal formation, as previously observed for Pd/CuCIP. The FE-SEM characterisation shown in **Figure S4** put in evidence the formation of snowflake-shaped Rb_3PO_4 crystals in the Au_1Pd_1/CuCIP sample and a significantly higher concentration in the Au_1Pd_4/CuCIP sample. This is accomplished by ATR-FTIR measurements which showed the formation of bands at 1190, 1090, 900 cm^{-1} due to Rb_3PO_4.[33,34] These bands decrease in intensity when Pd loading was increased, as shown in **Figure S5**.

The Raman spectra for the CuCIP framework and Au_xPd_y/CuCIP catalysts were compared with monometallic Au/CuCIP and Pd/CuCIP as shown in **Figure S6**. Several peaks above 400 cm^{-1} were obtained corresponding to the $P_2O_7^{2-}$ unit in the CuCIP framework.[35] Upon increasing the concentration of Au, the appearance of two new bands at 343 and 320 cm^{-1} was observed and ascribed to the antisymmetric and symmetric Au-Cl vibrations of $[AuCl_4]^-$ ions. A similar trend was observed for $[PdCl_4]^-$ as for the formation of two new bands at 298 and 197 cm^{-1} due to Pd-Cl symmetric stretching and Cl-Pd-Cl bending modes.[36] The appearance of one single broad band when the Au loading was low or absent could be caused by the reduced framework stability, as already highlighted by X-ray powder diffraction analysis.

The as synthesized catalysts appeared coloured and displayed absorption bands in the UV-Vis-NIR range. More in detail, the CuCIP framework (**Figure 7** (a), black line) exhibited typical bands at 44000 cm^{-1}, 35300 cm^{-1} and 26500 cm^{-1} due to the charge transfer transitions between Cu^{II} and Cl atoms.[24,37] Moreover, the copper (II) d-d transitions were observed at lower wavelengths. Particularly, the absorption band at 11850 cm^{-1} is related to d-d electronic transition of copper coordinated to chlorine as $[CuCl_4]^{2-}$ ions with a square planar geometry located within the D1 channels of the framework.[24,37] The absorption at 9900 cm^{-1} can be associated to the copper d-d transition of polyhedral $Cu^{II}O_4$ species where the chloride ions were located at the apex of CuO_4Cl square-based pyramids of the framework and Cu (II) has a tetrahedral coordination.[24,37]

The composition ratio of Au and Pd also affected the electronic properties of the catalysts. Indeed, bands at 34300 and 19200 cm^{-1} were ascribed to the $[PdCl_4]^{2-}$ complex[38] which likely increased in intensity with the increase of the Pd amount and at 32250 cm^{-1} to the charge transfer Au(III)-Cl of $[AuCl_4]^{2-}$.[39,40] These features further confirmed the presence of precursors within the microporous channels of the framework. As a matter of fact, the absorption at 18500 cm^{-1} due to LSPR excitation of $Au^{[19,41]}$ was observed on the reduced Au/CuCIP catalyst, as shown in **Figure S7**. In this frame, the spectra of the as synthesized and reduced Au_1Pd_1/CuCIP catalyst displayed interesting features, according to **Figure 7** (b). Indeed, a decrease in intensity of the absorption at 26500 cm^{-1} due to the charge transfer transitions between Cu^{II} and Cl atoms[24,37] accompanied by the simultaneous decrease in intensity of the bands at 19200 cm^{-1} due to the $[PdCl_4]^{2-}$ complex [36] and at 32250 cm^{-1} due to $[AuCl_4]^{2-}$.[37,38] were observed upon reduction. The findings indicate the decomposition of both metal precursors to form metal NPs with some modification of the CuCIP framework. Nevertheless, differently from what observed for Au/CuCIP, no absorption related to the LSPR excitation of $Au^{[19,41]}$ was detected in the case of the Au_1Pd_1/CuCIP catalyst, which indicates that an electronic interaction between the two metals is occurring after reduction. The absence of the Au plasmon band could indicate the formation of an alloy between the two metals, in agreement with the EDS characterisation results. An exponentially increasing absorbance towards higher energy has been reported as a consequence of interband transitions related to the formation of bimetallic particles.[42]
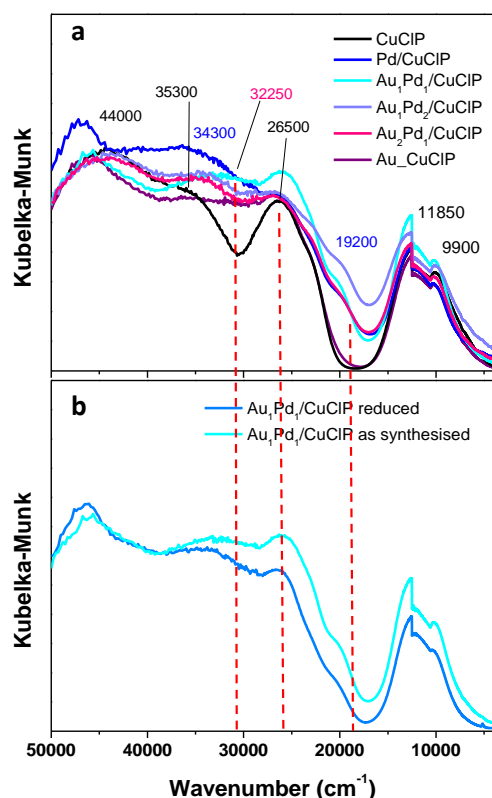
Figure 7. (a) DR UV-Vis-NIR spectra of the as synthesized catalysts. The spectrum of the CuClP framework is reported for comparison purposes. (b) DR UV-Vis-NIR spectra of the as synthesized (cyan line) and reduced (blue line) Au_1Pd_1/CuClP catalyst. The dashed red lines have been reported as eye guidelines.

With the aim to exploit the optical absorption property of the prepared samples, the plasmonic catalytic reaction over Au_xPd_y/CuClP was carried out in the Suzuki-Miyaura coupling reaction under visible light irradiation.

Plasmon-mediated catalysis: Suzuki-Miyaura coupling reaction

The plasmonic catalysis activity via synthesis of Pd-based bimetallic systems has been reported to have a significant effect on enhancing the catalytic and photocatalytic activity.[28,43–45] Under light irradiation conditions, the hot electrons generated by the LSPR effect can be used to activate the organohalide by the electron-transfer mechanism.[46,47] The computational density functional theory (DFT) calculations have also shown the elongation of the C-X bond as a result of the electron transfer; confirming the activation of the reactant.[48] This section describes the Suzuki-Miyaura coupling reaction results over Au_xPd_y/CuClP samples and their comparative study in dark and under visible light irradiation. **Figure 8a** summarizes the obtained catalytic performance of Au_xPd_y/CuClP catalysts between iodobenzene and phenylboronic acid under dark conditions. The active site for this reaction is Pd, as monometallic Au/CuClP did not display any product yield. The monometallic Pd/CuClP catalyst showed considerable activity in the reaction. It achieved a biphenyl yield

of ca. 27% after 4 h. The addition of Au in the catalyst had the effect of improving the yield even under dark conditions. Both the Au_1Pd_2/CuClP and Au_1Pd_1/CuClP catalysts generated higher yields of biphenyl. In the case of Au_1Pd_2/CuClP, the yield was marginally higher at ca. 30% after 4 h. The biphenyl yield that was produced by the bimetallic Au_1Pd_1/CuClP catalyst was significantly higher than the monometallic Pd/CuClP catalyst. The bimetallic catalyst achieved a yield of ca. 36% (TON = 20), a 33% increase compared to the Pd/CuClP (TON =13). This increase was noteworthy considering that the Pd content of the Au_1Pd_1/CuClP catalyst was lower than that of the Pd/CuClP catalyst (**Table S1**). It was also indicative of Au playing a role in promoting the activity of the Pd in the catalyst. The promoting effect was indisputable only in the Au_1Pd_1/CuClP catalyst, suggesting that perhaps the Au:Pd ratio greatly influenced the extent to which the Pd was promoted by Au.[22] The higher activity of the Au_1Pd_1/CuClP catalyst compared to the Pd/CuClP justified making the bimetallic catalyst the focus of further catalytic studies.

The initial substituent effect studies were performed with halogen-substituted benzene. The catalytic activity of the Au_1Pd_1/CuClP catalyst in the coupling reaction is shown in **Figure 8b**. The observed sequence of biphenyl yield was I>Br>Cl. This was in line with the activity of the halogen substituents as reported in the literature. The Au_1Pd_1/CuClP was therefore a reliable system, as its trend of activity was consistent with predictions from the literature. Further substituent effects analysis was done by using para-substituted Iodobenzene (**Figure 8c**) as iodobenzene produced the highest biaryl yield amongst all the halobenzenes.
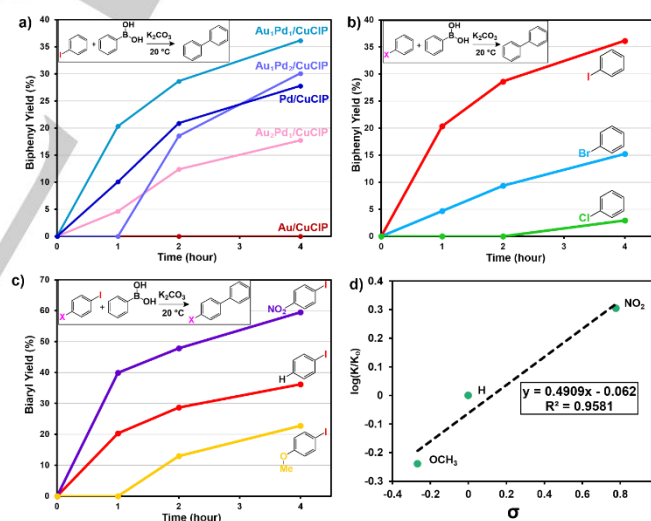

Figure 8. a) Activity of Au_xPd_y/CuClP catalysts in the Suzuki-Miyaura coupling of iodobenzene and phenylboronic acid. b) Activity of Au_1Pd_1/CuClP catalyst in the Suzuki coupling of halobenzenes and phenylboronic acid. c) Activity of Au_1Pd_1/CuClP catalyst in the Suzuki c) Activity of Au_1Pd_1/CuClP catalyst in the Suzuki coupling of para-substituted iodobenzene and phenylboronic acid. d) Hammett plot of the Suzuki coupling of para-substituted iodobenzene and phenylboronic acid. All reactions were done in dark conditions.

The activating effect of electron-withdrawing para-substituted-NO_2 was quite pronounced. The biaryl yield when the p-iodonitrobenzene was coupled with phenylboronic acid was ca. 60%, this indicated a 40 % increase in yield. It was clear that the maximum yield of biaryl that could be produced by the

Au_1Pd_1/CuCIP catalyst could be amplified by the addition of electron-withdrawing substituents. As predicted from the literature and theory of substituent effect, the effect of electron-donating para-substituted $-OCH_3$ was a lower yield (ca. 23 %) of the biaryl product.

The substituent effect was quantified using kinetic parameters of the Au_1Pd_1/CuCIP catalyst generated from a Hammett plot of the substituted iodobenzene (**Figure 8d**). The kinetic parameters were calculated based on pseudo-first-order kinetics with respect to the para-substituted iodobenzene as the phenylboronic acid was in ca. 10% molar excess. The reaction constant ρ determined from the Hammett plot was 0.49.[49] The positive value of the slope was indicative of the reaction being accelerated by the para-substituted electron-withdrawing group. The acceleration was due to the generation of a transition state in which the negative charge in the aryl ring was stabilized by the catalyst.
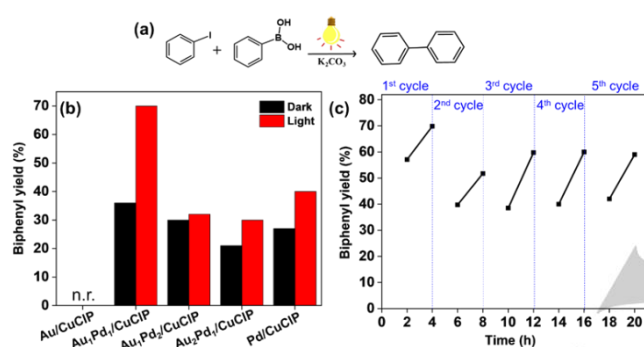

Figure 9. a) Suzuki-Miyaura coupling reaction, (b) Comparison of biphenyl product formation by Au_xPd_y/CuCIP catalysts in dark and under light irradiation conditions, (c) Recycling stability test using Au_1Pd_1/CuCIP catalyst under visible light irradiation conditions.

The investigation of catalytic activity under visible light irradiation was then carried out (**Figure 9a**) and compared with the amount of product formation in dark conditions as summarized in **Figure 9 (b)**. The most active catalyst in dark conditions, Au_1Pd_1/CuCIP, also displayed superior catalytic performance under visible light irradiation conditions. Furthermore, the enhancement factor was also found to be highest when compared with other catalysts with different ratios of Au and Pd. The monometallic Au did not display any activity with light irradiation, similar to dark conditions however, in contrast, monometallic Pd/CuCIP displays enhanced activity under light conditions, in line with expectations. The obtained biphenyl product yield of 70 % was nearly two times higher than the result obtained in dark conditions (36% yield). This enhancement factor was also the highest amongst varied ratios of Au and Pd incorporated in the CuCIP framework. In addition, to further optimize the ratio of Au and Pd in the CuCIP framework, 1:4 and 4:1 compositions of catalysts were prepared and investigated for their catalytic performance. An inferior biphenyl product yield of 16 % and 22 % was obtained with Au_1Pd_4/CuCIP and Au_4Pd_1/CuCIP, respectively under visible light irradiation conditions. The combination of Pd_1Pt_1 catalyst incorporated in the CuCIP framework also displayed an inferior product yield of 18 % (**Figure S8**). Moreover, the action spectrum of Au_1Pd_1/CuCIP with

different wavelengths of light irradiation displayed superior product yields in the region of Au LSPR absorption at 19400 cm^{-1} (~515 nm) as shown in **Figure S9**. This observation confirmed the product yield enhancement due to the plasmonic absorption of Au NPs. A control experiment in dark at 40° C was performed to study the influence of rise in temperature during the light irradiation conditions (**Figure S10**). The inferior product yield obtained under thermal conditions prove the key role of light irradiation in enhancing the product yield.

The recycling ability of the catalyst was tested by recovering the catalyst by simple centrifugation and re-starting the reaction with the addition of fresh substrates. The obtained stability result of Au_1Pd_1/CuCIP under visible light irradiation is shown in **Figure 9 (c)**. The catalytic activity displayed a drop in 10 % product yield at the end of the 3rd cycle (mostly due to handling losses). These catalysts can be recovered by a very simple procedure without any significant loss of catalytic performance. The characterization of reused catalyst was investigated by XRD and FE-SEM analysis. **Figure S11** displays the XRD pattern distinctive of the CuCIP framework of the fresh and re-used Au_1Pd_1/CuCIP catalyst. The XRD diffraction spectra did not display any changes in the peak positions. The development of additional peaks at 25° which ascribes to the sintering of the framework or the formation of Rb_3PO_4 phases was also found to be absent. **Figure 6e** also shows the FE-SEM image of the recovered catalyst which did not display any significant morphological changes. The EDS spectra revealed the presence of Au and Pd NPs on the surface of the catalyst, especially the existence of small-sized Pd NPs. Such behavior was consistent with the EDS analysis spectra obtained on the fresh Au_1Pd_1/CuCIP catalyst. Furthermore, other impurities such as K_2CO_3 used during the catalytic reaction were also evidenced.

Feng et al. have investigated the mechanism of hot-electron-induced Suzuki-Miyaura coupling reaction over AuPd NPs by surface-enhanced Raman spectroscopic measurements.[47] Upon light irradiation, the hot electrons generated on the surface of bimetallic NPs due to the Au plasmonic excitation get transferred to the adsorbed substrate species, thereby assisting in the cleavage of the C-X bond.[19,50–52] The reaction then proceed by transmetalation and reductive elimination to form the final product, biphenyl, as illustrated in **Figure S12**. The distinct nature of Au and Pd NPs on the surface of the CuCIP framework displaying the feature of LSPR can be further developed to enhance the catalytic and photocatalytic transformations in diverse reactions.

Conclusions

In conclusion, different ratios of Au and Pd NPs on the CuCIP support framework were prepared by an extrusion method and investigated for their catalytic and photocatalytic performance under visible light irradiation conditions. Amongst all, Au_1Pd_1 catalyst supported on CuCIP support framework displayed the superior catalytic activity in dark conditions and the highest plasmonic enhancement factor under visible light irradiation. Nearly, a two-fold enhancement in the product yield was observed with Au_1Pd_1/CuCIP catalyst. This is the first time, CuCIP microporous support framework has been utilized to explore the

visible-light-driven catalytic activity in the Suzuki-Miyaura coupling reaction. The presence of different substituents (EDG and EWG) on aryl halide was also investigated to study the effect on the amount of product formation. We expect that this report will further spark a new interest in the exploration of unique materials to design efficient catalytic and photocatalytic systems.

Experimental Section

Materials: All chemicals were used as received without any further purification.

Synthesis of CuClP and Au_xPd_y/CuClP: Copper (II) fluoride (1.725 mmol), RbCl (3.474 mmol), and K_xMCl_4 (0.216 mmol) were grounded by agate pestle and mortar to ensure adequate mixing of the reagents. The solid mixture was then placed in the polytetrafluoroethylene (PTFE) liner of a custom-made 23 cm^3 hydrothermal vessel. The orthophosphoric acid (85 wt.%; 360 μL) was added dropwise wetting all the content followed by ultrasonication for 10 minutes to create uniform dispersion. Next, RbOH (50 wt.%; 300 μL) was added and ultrasonicated for another 10 minutes. The mixture was then treated hydrothermally at 175 ℃ for 48 h. The products were formed as cuboid crystals, which were green in color for the Au/CuClP material and brown for the Pd/CuClP. The colors of the bimetallic catalysts were some combination of the monometallic. The materials were further activated by reduction under 5% H_2/N_2 for 2 h at 200 ℃ to generate the active catalysts. After calcination, the materials appeared darker in color. The Au:Pd ratio in K_xMCl_4 (where M = Au, Pd) was altered to obtain the stated nominal loadings. The different prepared catalysts were: blank CuClP framework, Au/CuClP, Pd/CuClP, Au_1Pd_1/CuClP, Au_1Pd_2/CuClP, Au_2Pd_1/CuClP, Au_1Pd_4/CuClP and Au_4Pd_1/CuClP. For the undoped CuClP material, copper (II) fluoride replaced the K_xMCl_4 salts. For the sake of clarity, the bimetallic catalysts will be also indicated as Au_xPd_y/CuClP.

Characterization:
The powder X-ray diffraction (XRD) patterns were collected by using a Bruker D2 phaser diffractometer using Cu K α1 radiation.
XPS measurements were performed at Harwell XPS, which is an EPSRC national facility in the UK.
Pd K-edge and Au L_3-edge XAS studies were measured on the B18 beamline at the Diamond Light Source as part of our membership of the UK Catalysis Hub Beamtime Allocation Group.
FESEM (Field Emission Scanning Electron) measurements were performed using a Tescan S9000G FESEM 3010 microscope (30 kV) equipped with a high brightness Schottky emitter and fitted with Energy Dispersive X-ray Spectroscopy (EDS) analysis by an Ultim Max Silicon Drift Detector (SDD, Oxford). For analyses, the samples, in the form of powders, were deposited on a stub coated with a conducting adhesive and inserted in the chamber by a fully motorised procedure.
HR-TEM analysis was performed using Jeol JEM 3010 (300 kV) microscope equipped with a LaB_6 filament and fitted with X-ray EDS analysis by a Link ISIS 200 detector. For the analyses, the powdered sample was deposited on a copper grid, coated with a porous carbon film. All digital micrographs were acquired with an Ultrascan 1000 camera and the images were processed by Gatan digital micrograph. Metal particle size distribution and mean particle diameter (d_m) of copper-containing nanoparticles were obtained by considering a statistically representative number of particles (specificare inserendo il numero arrotondato) on several images. The d_m was calculated using the following equation (1):
$$d_m = \Sigma d_i n_i / \Sigma n_i \quad (1)$$
where n_i is the number of particles of diameter d_i.
Micro Raman spectra were recorded with a Horiba Jobin Yvon HR800 spectrometer, equipped with an Olimpus BX41 microscope, by exciting with a 532 nm laser. The spectra were collected in air.
ATR (Attenuated Total Reflection) spectra were obtained on pure samples with a Bruker Vertex 70 spectrophotometer equipped with Harrick MVP2

ATR cell and DLaTGS detector (32 scan, 4 cm^{-1} resolution). The spectra were collected in air.
The metal content was determined by ICP analysis using a high-resolution inductively coupled plasma-mass spectrometer (MS) Thermo Scientific ELEMENT 2XR (Waltham, MA, USA), with appropriate standards for quantification.
Diffuse reflectance (DR) UV-Vis-NIR characterisation was performed on the samples in the form of powders placed in a quartz cell and the spectra were run on a Varian Cary 5000 spectrophotometer, working in the range of wavenumbers 4000 - 50000 cm^{-1} (200 – 2500 nm). The DR UV-Vis-NIR spectra were recorded in air, at room temperature and without any previous activation and reported in the Kubelka-Munk function (F) as shown in equation (2):
$$F(R_\infty) = \frac{(1 - R_\infty)^2}{2R_\infty} = \frac{K}{s} \quad (2)$$
where R_∞ is the reflectance of a hypothetical infinitely thick layer of the sample. K is the molar absorption coefficient and s is the scattering coefficient.
Clarus 480 gas chromatograph equipped with a flame ionization detector and Elite 5 column was used to analyze reaction products employing biphenyl as an external standard reagent for Suzuki-Miyaura coupling reaction. LOT LS0104 solar simulator fitted with a 150 W Xenon light source was used to conduct a reaction under visible light irradiation conditions.

Catalytic activity test

Suzuki-Miyaura coupling reaction: The Suzuki coupling reaction between phenylboronic acid and iodobenzene (or other substrates) was carried out by using a suspension of the catalyst in 15 ml of ethanol. 50 mg of the catalyst, along with 124.5 mg of K_2CO_3 mild base and 109.8 mg of phenylboronic acid were weighed in a 50 ml Pyrex round bottom flask. 115.3 mg of naphthalene was added to the mixture and used as an external standard for GC quantification of the product formation. Finally, 111.5 μL (1.0 mmol) of iodobenzene (or other substrates) was added to initiate the reaction and stirred continuously in dark or under visible light irradiation conditions (λ > 420 nm) for 4 h.

Acknowledgments

[1]   P. Verma, K. Mori, Y. Kuwahara, R. Raja, H. Yamashita, *Mater. Adv.* **2021**, *2*, 880–906.
[2]   X. Zhang, Y. Fan, E. You, Z. Li, Y. Dong, L. Chen, Y. Yang, Z. Xie, Q. Kuang, L. Zheng, *Nano Energy* **2021**, *84*, 105950.
[3]   J. Becerra, D. T. Nguyen, V. N. Gopalakrishnan, T. O. Do, *ACS Appl. Energy Mater.* **2020**, *3*, 7659–7665.
[4]   G. Kumari, X. Zhang, D. Devasia, J. Heo, P. K. Jain, *ACS Nano* **2018**, *12*, 8330–8340.

[5]   P. Verma, Y. Kuwahara, K. Mori, H. Yamashita, *Catal. Sci. Technol.* **2017**, *7*, 2551–2558.

[6]   P. Verma, Y. Kuwahara, K. Mori, R. Raja, H. Yamashita, *EnergyChem* **2022**, *4*, 100070.

[7]   Z. Zhang, A. Li, S.-W. Cao, M. Bosman, S. Li, C. Xue, *Nanoscale* **2014**, *6*, 5217–5222.

[8]   Z. Zheng, T. Tachikawa, T. Majima, *J. Am. Chem. Soc.* **2014**, *136*, 6870–6873.

[9]   Z. Lou, Q. Gu, L. Xu, Y. Liao, C. Xue, *Chem. Asian J.* **2015**, *10*, 1291–1294.

[10]   R. Li, W. H. Cheng, M. H. Richter, J. S. Duchene, W. Tian, C. Li, H. A. Atwater, *ACS Energy Lett.* **2021**, *6*, 1849–1856.

[11]   K. M. Kamal, R. Narayan, N. Chandran, S. Popović, M. A. Nazrulla, J. Kovač, N. Vrtovec, M. Bele, N. Hodnik, M. M. Kržmanc, B. Likozar, *Appl. Catal. B* **2022**, *307*, 121181.

[12]   R. Brisbin, J. Zhou, T. Bond, L. Voss, A. J. Simon, R. Baxter, A. S. P. Chang, *Journal of Physical Chemistry C* **2021**, *125*, 9730–9735.

[13]   Q. Gu, Q. Jia, J. Long, Z. Gao, *ChemCatChem* **2019**, *11*, 669–683.

[14]   D. Han, Z. Bao, H. Xing, Y. Yang, Q. Ren, Z. Zhang, *Nanoscale* **2017**, *9*, 6026–6032.

[15]   Z. Li, Y. Gong, X. Zhang, Y. Wen, J. Yao, M. Hu, M. He, J. Liu, R. Li, F. Wang, C. Zhang, *Nano Res.* **2020**, *13*, 2812–2818.

[16]   P. Verma, K. Mori, Y. Kuwahara, M. Manzoli, S. Morandi, C. Fukuhara, R. Raja, H. Yamashita, *ChemCatChem* **2023**, 15, e202201182.

[17]   M. Tahir, *Appl. Catal. B* **2017**, *219*, 329–343.

[18]   C. S. L. Koh, H. Y. F. Sim, S. X. Leong, S. K. Boong, C. Chong, X. Y. Ling, *ACS Mater. Lett.* **2021**, *3*, 557–573.

[19]   P. Verma, Y. Kuwahara, K. Mori, H. Yamashita, *J. Mater. Chem. A* **2016**, *4*, 10142–10150.

[20]   P. Verma, Y. Kuwahara, K. Mori, H. Yamashita, *Bull. Chem. Soc. Jpn.* **2019**, *92*, 19–29.

[21]   C. S. Hinde, A. M. Gill, P. P. Wells, T. S. Andy Hor, R. Raja, *ChemPlusChem* **2015**, *80*, 1226–1230.

[22]   C. S. Hinde, D. Ansovini, P. P. Wells, G. Collins, S. van Aswegen, J. D. Holmes, T. S. Andy Hor, R. Raja, *ACS Catal.* **2015**, *5*, 3807–3816.

[23]   A. M. Gill, C. S. Hinde, R. K. Leary, M. E. Potter, A. Jouve, P. P. Wells, P. A. Midgley, J. M. Thomas, R. Raja, *ChemSusChem* **2016**, *9*, 423–427.

[24]   M. Manzoli, A. Jouve, A. M. Gill, G. Cravotto, R. Raja, *J. Mater. Chem. A* **2018**, *6*, 14410–14419.

[25]   X. Huang, Y. Li, Y. Chen, H. Zhou, X. Duan, Y. Huang, *Angew. Chem. Int. Ed.* **2013**, *52*, 6063–6067.

[26]   S. Zhang, M. Li, J. Zhao, H. Wang, X. Zhu, J. Han, X. Liu, *Appl. Catal. B* **2019**, *252*, 24–32.

[27]   Z. Yong, Q. Shi, R. Fu, W. Cheng, *Adv. Mater. Interfaces* **2021**, *8*, 2001686.

[28]   F. Wang, C. Li, H. Chen, R. Jiang, L. D. Sun, Q. Li, J. Wang, J. C. Yu, C. H. Yan, *J. Am. Chem. Soc.* **2013**, *135*, 5588–5601.

[29]   J. Radnik, C. Mohr, P. Claus, *Phys. Chem. Chem. Phys.* **2003**, *5*, 172–177.

[30]   J. T. Miller, A. J. Kropf, Y. Zha, J. R. Regalbuto, L. Delannoy, C. Louis, E. Bus, J. A. van Bokhoven, *J. Catal.* **2006**, *240*, 222–234.

[31]   X. Chen, X. Chen, Z. Cai, M. Oyama, *J. Mater. Chem. A* **2014**, *2*, 5668–5674.

[32]   C. S. Hinde, S. van Aswegen, G. Collins, J. D. Holmes, T. S. Andy Hor, R. Raja, *Dalton Trans.* **2013**, *42*, 12600–12605.

[33]   A. Jouini, M. Férid, M. Trabelsi-Ayadi, *Thermochim. Acta* **2003**, *400*, 199-204.

[34]   J. Zhu, H. Chen, Y. Zheng, H. L. Kong, W. D. Cheng, Y. de Wang, H. T. Guan, Z. Q. Zhu, *Rare Met.* **2015**, *34*, 877–881.

[35]   L. v. Stepakova, M. Y. Skripkin, L. v. Chernykh, G. L. Starova, L. Hajba, J. Mink, M. Sandström, *J. Raman Spectrosc.* **2008**, *39*, 16–31.

[36]   Y. Chen, D. H. Christensen, O. F. Nielsen, J. Hyldtoft, C. J. H. Jacobsen, *Spectrochim. Acta A Mol. Biomol. Spectrosc.* **1995**, *51*, 595–602.

[37]   C. Amuli, M. Elleb, J. Meullemeestre, M.-J. Schwing, F. Vierling, *Inorg. Chem.* **1986**, *25*, 856-861.

[38]   D. Tessier, A. Rakai, F. Bozon-Verduraz, *J. Chem. Soc. Faraday Trans.* **1992**, *88*, 741-749.

[39]   J. A. Peck, C. Drew Tait, B. I. Swanson, G. E. Brown Jr, *Geochim. Cosmochim. Acta* **1991**, *55*, 671-676.

[40]   T. M. Salama, T. Shido, R. Ohnishi, M. Ichikawa, *J. Phys. Chem.* **1996**, *100*, 3688-3694.

[41]   A. Villa, N. Dimitratos, C. E. Chan-Thaw, C. Hammond, G. M. Veith, D. Wang, M. Manzoli, L. Prati, G. J. Hutchings, *Chem. Soc. Rev.* **2016**, *45*, 4953–4994.

[42]   P. Dash, N. A. Dehm, R. W. J. Scott, *J. Mol. Catal. A Chem* **2008**, *286*, 114–119.

[43]   Y. T. Hung, M. T. Chen, M. H. Huang, T. Y. Kao, Y. S. Liu, L. C. Liang, *Inorg. Chem. Front.* **2014**, *1*, 405–413.

[44]   M. B. Thathagar, J. Beckers, G. Rothenberg, *J. Am. Chem. Soc.* **2002**, 124, 11858-11859.

[45]   P. Verma, Y. Kuwahara, K. Mori, H. Yamashita, *J. Mater. Chem. A* **2015**, *3*, 18889–18897.

[46]   Z. Li, D. Kurouski, *Nanophotonics* **2021**, *10*, 1657–1673.

[47]   H. S. Feng, F. Dong, H. S. Su, M. M. Sartin, B. Ren, *J. Appl. Phys.* **2020**, *128*, 173105.

[48]   Q. Xiao, S. Sarina, E. Jaatinen, J. Jia, D. P. Arnold, H. Liu, H. Zhu, *Green Chem.* **2014**, *16*, 4272–4285.

[49]   L. P. Hammett, *J. Am. Chem. Soc.* **1937**, *59*, 96–103.

[50]   S. T. Kochuveedu, Y. H. Jang, D. H. Kim, *Chem. Soc. Rev.* **2013**, *42*, 8467–8493.

[51]   B. Yan, S. v. Boriskina, B. M. Reinhard, *J. Phys. Chem. C* **2011**, *115*, 24437–24453.

[52]   M. Wang, M. Ye, J. Iocozzia, C. Lin, Z. Lin, *Adv. Sci.* **2016**, *3*, 1600024.

Entry for the Table of Contents

FULL PAPER
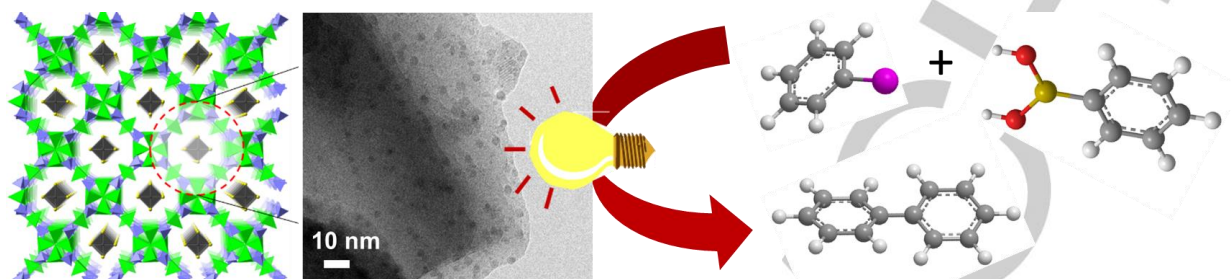
An extrusion method was employed to prepare AuPd bimetallic nanoparticles on a microporous CuCIP framework. These bimetallic nanoparticles were characterized by spectroscopic techniques to understand the structural and electronic modification with different metal ratios and correlated to its optimized plasmon-mediated enhanced catalysis under visible light irradiation.

Au_xPd_y-based heterogeneous nanocatalysts for plasmon-mediated enhanced catalysis under visible light irradiation

Priyanka Verma, Panashe M. Mhembere, Paolo Tallone, Maela Manzoli, Giuseppina Cerrato, Ryo Watanabe, Choji Fukuhara, Robert Raja and Hiromi Yamashita

Page No. – Page No.